Author/s:
Kim, C-J;Ercole, F;Chen, J;Pan, S;Ju, Y;Quinn, JF;Caruso, F

Title:
Macromolecular Engineering of Thermoresponsive Metal-Phenolic Networks

Date:
2022-01-01

Citation:
Kim, C. -J., Ercole, F., Chen, J., Pan, S., Ju, Y., Quinn, J. F. & Caruso, F. (2022). Macromolecular Engineering of Thermoresponsive Metal-Phenolic Networks. JOURNAL OF THE AMERICAN CHEMICAL SOCIETY, 144 (1), pp.503-514. https://doi.org/10.1021/jacs.1c10979.

Persistent Link:
https://hdl.handle.net/11343/295989

Macromolecular Engineering of Thermoresponsive Metal–Phenolic Networks

Chan-Jin Kim,[†] Francesca Ercole,[‡] Jingqu Chen,[†] Shuaijun Pan,[†] Yi Ju,[†] John F. Quinn,*[,‡,#] and Frank Caruso*[,†]

[†]Department of Chemical Engineering, The University of Melbourne, Parkville, Victoria 3010, Australia

[‡]Drug Delivery, Disposition and Dynamics Theme, Monash Institute of Pharmaceutical Sciences, Monash University, Parkville, Victoria 3052, Australia

[#]Department of Chemical Engineering, Faculty of Engineering, Monash University, Clayton, Victoria 3800, Australia

*Corresponding authors. Email: fcaruso@unimelb.edu.au (F.C.); john.f.quinn@monash.edu (J.F.Q.)

KEYWORDS: MPNs, Capsules, Thermoresponsive Properties, Permeability, Cargo Release

ABSTRACT

Dynamic nanostructured materials that can react to physical and chemical stimuli have attracted interest in the biomedical and materials science fields. Metal–phenolic networks (MPNs) represent a modular class of such materials: these networks form via coordination of phenolic molecules with metal ions and can be used for surface and particle engineering. To broaden the range of accessible MPN properties, we report the fabrication of thermoresponsive MPN capsules using Fe^{III} ions and the thermoresponsive phenolic building block biscatechol-functionalized poly(*N*-isopropylacrylamide) (biscatechol-PNIPAM). The MPN capsules exhibited reversible changes in capsule size and shell

thickness in response to temperature changes. The temperature-induced capsule size changes were influenced by the chain length of biscatechol-PNIPAM and catechol-to-Fe^{III} ion molar ratio. The metal ion type also influenced the capsule size changes, allowing tuning of the MPN capsule mechanical properties. Al^{III}-based capsules, having a lower stiffness value (10.7 mN m^{-1}), showed a larger temperature-induced size contraction (~63%) than Tb^{III}-based capsules, which exhibit a higher stiffness value (52.6 mN m^{-1}) and minimal size reduction (<1%). The permeability of the MPN capsules was controlled by changing the temperature (25–50 °C)—a reduced permeability was obtained as the temperature was increased above the lower critical solution temperature of biscatechol-PNIPAM. This temperature-dependent permeability behavior was exploited to encapsulate and release model cargo 500 kDa fluorescein isothiocyanate-tagged dextran from the capsules; approximately 70% was released over 90 min at 25 °C. This approach provides a synthetic strategy for developing dynamic and thermoresponsive-tunable MPN systems for potential applications in biological science and biotechnology.

INTRODUCTION

Stimuli-responsive materials that can respond to specific triggers are of interest in a range of applications such as drug delivery,[1,2] diagnostics,[3] biomedical devices,[4] self-healing materials,[5] catalysis,[6] membranes,[7] and the development of micro/nanoreactors.[8,9] Such materials can be designed to respond to various stimuli such as pH,[10,11] redox potential difference,[12] enzymes,[13,14] nucleic acids,[15] temperature,[16,17] light,[18] ultrasound,[19] or magnetic fields.[20,21] The application of, or exposure to, such stimuli can result in expansion or contraction, assembly or disassembly, degradation or aggregation, morphology changes or cargo encapsulation or release.[22] Thermoresponsive polymers are often exploited in stimuli-responsive systems due to their sharp temperature-dependent phase transition behaviors. Various synthetic polymers featuring thermoresponsive properties display discrete lower critical solution or upper critical solution temperatures (LCSTs or UCSTs), which can be tuned from 0 to 100 °C by varying the structure of the polymer.[23]

PNIPAM is one of the most widely studied and applied thermoresponsive polymers and undergoes a reversible and sharp phase transition at approximately 32 °C. PNIPAM exists as a hydrophilic and fully hydrated chain below the LCST due to hydrogen bonding with surrounding water molecules.[23,24] Upon heating, intra- and intermolecular hydrogen bonding between the amide repeat units of the polymer becomes more favored than hydrogen bonding with the water molecules, resulting in the phase transition to a hydrophobic and dehydrated globule.[23,24] The LCST of PNIPAM can be readily tuned by incorporating hydrophilic or hydrophobic moieties, which makes PNIPAM a suitable component for developing smart responsive materials.[25,26] Such PNIPAM-based materials have been engineered to control nanoparticle aggregation behavior,[25,27] regulate binding properties to oligonucleotides, enzymes, and cells,[17,28] and undergo thermally induced reversible material shape changes.[12,16,29]

Metal–phenolic networks (MPNs) are an emerging class of metal–organic supramolecular assemblies and their formation is largely governed by the coordination between phenolic molecules and metal ions.[30,31] MPN films can be deposited on a broad range of substrates, from nanometer to centimeter-sized inorganic, organic, and biological materials.[30,31] MPNs have potential in a broad range of applications due to their versatile assembly process, strong adhesion to substrates, and negligible cytotoxicity.[30,32,33] Moreover, MPN-based multifunctional self-assembled nanoplatforms were recently developed for the inhibition of tumor proliferation and metastasis.[34,35] MPN systems prepared from commercially available phenolic molecules, such as tannic acid (TA), epigallocatechin gallate, gallic acid, and pyrocatechol, show responses to various stimuli including pH, light, and redox potential.[30,36–39] Expanding the suite of stimulus-responsive MPNs by integrating thermoresponsive polymers, such as PNIPAM, coupled with the modular nature of MPNs, is an attractive strategy for generating functional MPN films/capsules that are responsive to thermal stimuli.

Herein, we designed and synthesized thermoresponsive α,ω-biscatechol-functionalized PNIPAM [i.e., M_n = 6700 g mol^{-1} (repeat unit (n) = 55), 17 600 g mol^{-1} (n = 151), 27 300 g mol^{-1} (n = 237), 41

700 g mol^{-1} (n = 364)]. The synthesized PNIPAM chains were used as MPN building blocks for coordination with 18 different metal ions to obtain thermoresponsive MPN capsules. The prepared MPN capsules underwent reversible size changes with changes in the temperature below and above the LCST (i.e., 25 and 50 °C). The thermally induced size reduction of the capsules was tuned by varying either the molecular weight of PNIPAM or the ratio between the catechol groups and metal ions used for the MPN process. Moreover, by employing a binary mixture of metal ions at different ratios or through the selection of different metal ions, the thermoresponsive properties of the MPN capsules enabled their size to be broadly tuned (i.e., a reduction in size from ~1–68% upon heating from 25 to 50 °C). In addition, we demonstrate that the thermoresponsive MPN capsules show variable permeability, which was subsequently exploited to achieve thermally induced cargo (500 kDa fluorescein isothiocyanate-tagged dextran (FITC)-dextran) encapsulation and release in response to temperature changes. This study demonstrates the rational design and fabrication of thermoresponsive MPN capsules, which may be of broad interest in various applications that require species to be encapsulated and released at specific temperatures (e.g., confined chemical and biochemical reactions), and, when applied to specific polymers with LCST or UCST suitable for drug delivery, may provide a platform for engineering MPN capsules for therapeutic delivery applications.

Scheme 1. (a) Synthesis of Biscatechol-Functionalized Bis(carboxymethyl)trithiocarbonate (biscatechol-BCMT). (b) RAFT Polymerization of *N*-isopropylacrylamide (NIPAM) for Synthesis of Biscatechol-PNIPAM.

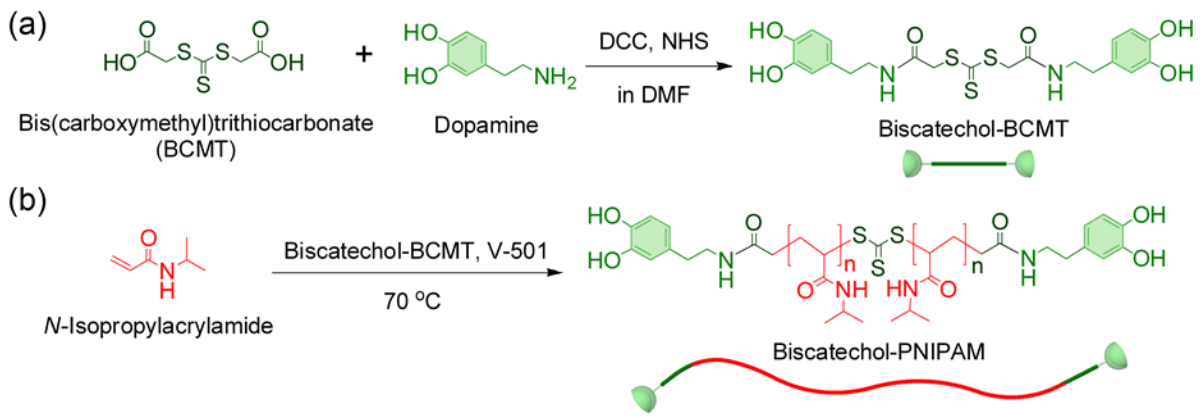

RESULTS AND DISCUSSION

Design and Synthesis of α,ω-Biscatechol-Functionalized PNIPAM. α,ω-Biscatechol-functionalized PNIPAM (biscatechol-PNIPAM) was synthesized by reversible addition–fragmentation chain transfer (RAFT) polymerization using a symmetrical trithiocarbonate chain transfer agent (CTA) with two catechol groups (Scheme 1). To synthesize the RAFT agent (biscatechol-functionalized bis(carboxymethyl)trithiocarbonate (biscatechol-BCMT)), BCMT was conjugated to dopamine via amide coupling with *N*,*N*′-dicyclohexylcarbodiimide (DCC) and *N*-hydroxysuccinimide (NHS) (Scheme 1a). The synthesized biscatechol-BCMT was purified by preparative high-performance liquid chromatography (HPLC) and characterized by analytical HPLC and nuclear magnetic resonance (NMR) spectroscopy (Figures S1 and S2). PNIPAM with catechol groups at both chain termini was then prepared by RAFT polymerization using the synthesized biscatechol-BCMT (CTA) and 4,4′-azobis(4-cyanopentanoic acid) (V-501, initiator) (Scheme 1b). Four polymers were synthesized: biscatechol-PNIPAM$_{55}$ (M_n = 6700 g mol^{-1}, repeat unit (n) = 55); biscatechol-PNIPAM$_{151}$ (M_n = 17 600 g mol^{-1}, n = 151); biscatechol-PNIPAM$_{237}$ (M_n = 27 300 g mol^{-1}, n = 237), and biscatechol-PNIPAM$_{364}$ (M_n = 41 700 g mol^{-1}, n = 364). The synthesized polymers were characterized by NMR and gel permeation chromatography (GPC) (Figures S3 and S4); the characterization data are provided in Table S1. As the GPC system was calibrated using polymethyl methacrylate standards, the determined molecular weights of biscatechol-PNIPAMs are relative values and do not reflect the true molecular weights of the synthesized polymers. Therefore, approximate number-average molecular weights for biscatechol-PNIPAM were calculated from the ^{1}H NMR data by comparing the integral of the peak at 2.63 ppm (from the conjugated dopamine moiety) with that at 4.00 ppm (from the polymer backbone) (Figure S3).

Scheme 2. (a) Schematic Illustration of the Preparation of Thermoresponsive MPN Capsules using Biscatechol-PNIPAM and Metal Ions. (b) Temperature-Triggered Control of Thermoresponsive MPN Capsules: Size, Shell Thickness, and Permeability.

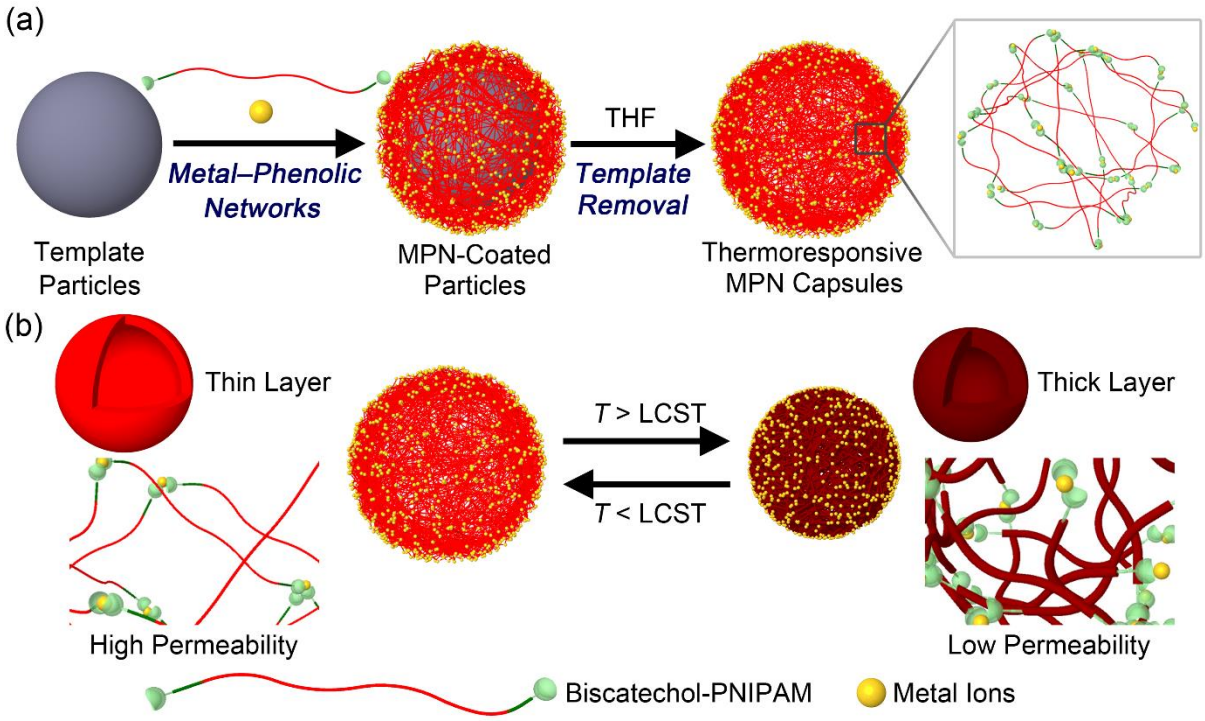

Fabrication of Thermoresponsive MPN Capsules. Metal ions and biscatechol-PNIPAM chains were used to form MPN films on sacrificial template particles (i.e., carboxylic acid-functionalized polystyrene (PS-COOH, 1.86 ± 0.03 μm) particles) (Scheme 2a). The template particles, dispersed in water, were mixed with biscatechol-PNIPAM solutions and $FeCl_3 \cdot 6H_2O$. 3-(*N*-Morpholino)propanesulfonic acid (MOPS) buffer (25 mM, pH 7.4) was then added to the suspension to raise the pH, resulting in bis- and tris-dominant coordination states between biscatechol-PNIPAM and Fe^{III} ions.[30] The adsorption of biscatechol-PNIPAM chains onto the template particles, and the subsequent network formation between the phenolic building blocks and metal ions occurs during this assembly procedure.[31,40,41] Thermoresponsive MPN capsules were then obtained by selectively dissolving the PS-COOH particles using tetrahydrofuran (THF). Such a dissolution process for PS is one we have commonly used, as exemplified elsewhere.[30] The resulting PNIPAM–Fe^{III} MPN capsules are expected to display reversible thermoresponsive behavior due to the incorporation of PNIPAM

chains into the capsule shell (Scheme 2b). Specifically, when the temperature is increased above the LCST, the conformation of PNIPAM changes from a water-swollen to a dehydrated state, resulting in reduction in size of the MPN capsules with a concomitant increase in shell thickness and a decrease in permeability.

$PNIPAM_{364}$–Fe^{III} MPN capsules prepared from biscatechol-$PNIPAM_{364}$, Fe^{III} ions, and PS-COOH particles were characterized by differential interference contrast (DIC) microscopy, scanning electron microscopy (SEM), transmission electron microscopy (TEM), atomic force microscopy (AFM), and high-angle annular dark-field (HAADF) microscopy (Figure 1). The images revealed well-dispersed capsules in solution, and folds and creases characteristic of collapsed capsule structures in the air-dried state. The shell thickness of the $PNIPAM_{364}$–Fe^{III} MPN capsules was 13.9 nm, as measured by AFM. Energy-dispersive X-ray spectroscopy (EDX) elemental mapping revealed that C, N, O, and Fe were all uniformly distributed throughout the $PNIPAM_{364}$–Fe^{III} MPN capsules, indicating that the capsules are composed of PNIPAM chains and Fe^{III} ions. The UV–vis spectrum of the $PNIPAM_{364}$–Fe^{III} MPN capsules featured a characteristic ligand-to-metal charge transfer (LMCT) band around 565 nm (Figure S5), which is indicative of the coordination between biscatechol-PNIPAM and Fe^{III} ions in the MPN capsules,[42,43] and specifically the presence of bis- and tris-type coordination between biscatechol-PNIPAM and Fe^{III} ions in the capsules, where the bis-state is dominant. The coordination between biscatechol-PNIPAM and Fe^{III} ions was influenced by pH change, corresponding to the transition between mono-, bis-, and tris-complex states (Figure S6).[30]

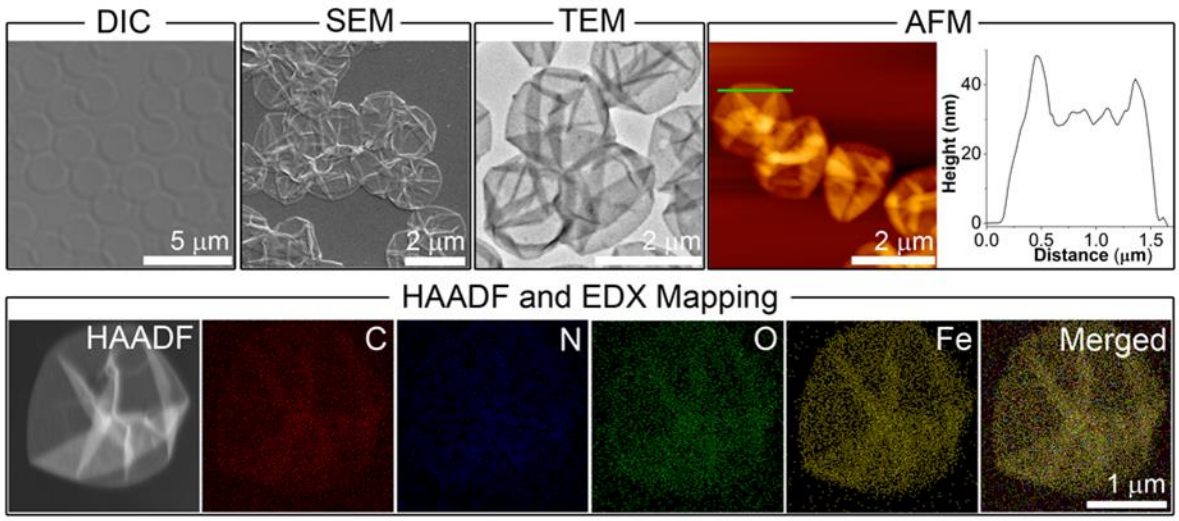

Figure 1. Characterization of PNIPAM$_{364}$–Fe^{III} MPN capsules using DIC, SEM, TEM, AFM, HAADF, and EDX elemental mapping. The height versus distance profile of an MPN capsule plotted along the green line in the AFM image is also shown.

Thermally Induced MPN Capsule Size Changes. The temperature-dependent size reduction of PNIPAM$_{364}$–Fe^{III} MPN capsules was monitored by dynamic light scattering (DLS) over the temperature range of 25–50 °C (Figure 2a). Although the LCST of biscatechol-PNIPAM$_{364}$ was determined to be 33.6 °C (which is within the typical LCST range of PNIPAM (30–35 °C))[24] (Figure S7), the size of the MPN capsules decreased continually when heated from 35 to 50 °C. The gradual reduction in size observed for the PNIPAM$_{364}$–Fe^{III} MPN capsules with increasing temperature has also been reported for other PNIPAM-based material systems.[44,45] Moreover, thermally induced contraction and expansion of the capsules was observed over several cycles (Figure 2b); the sizes of the PNIPAM$_{364}$–Fe^{III} MPN capsules were 2.3 ± 0.1 and 1.9 ± 0.1 μm at 25 and 50 °C, respectively, as calculated from DIC images (Figure 2c). These results demonstrate that the MPN capsules assembled via coordination chemistry between biscatechol-PNIPAM and Fe^{III} ions retain the thermoresponsive properties of the parent polymer, albeit with some difference in the apparent transition temperature.

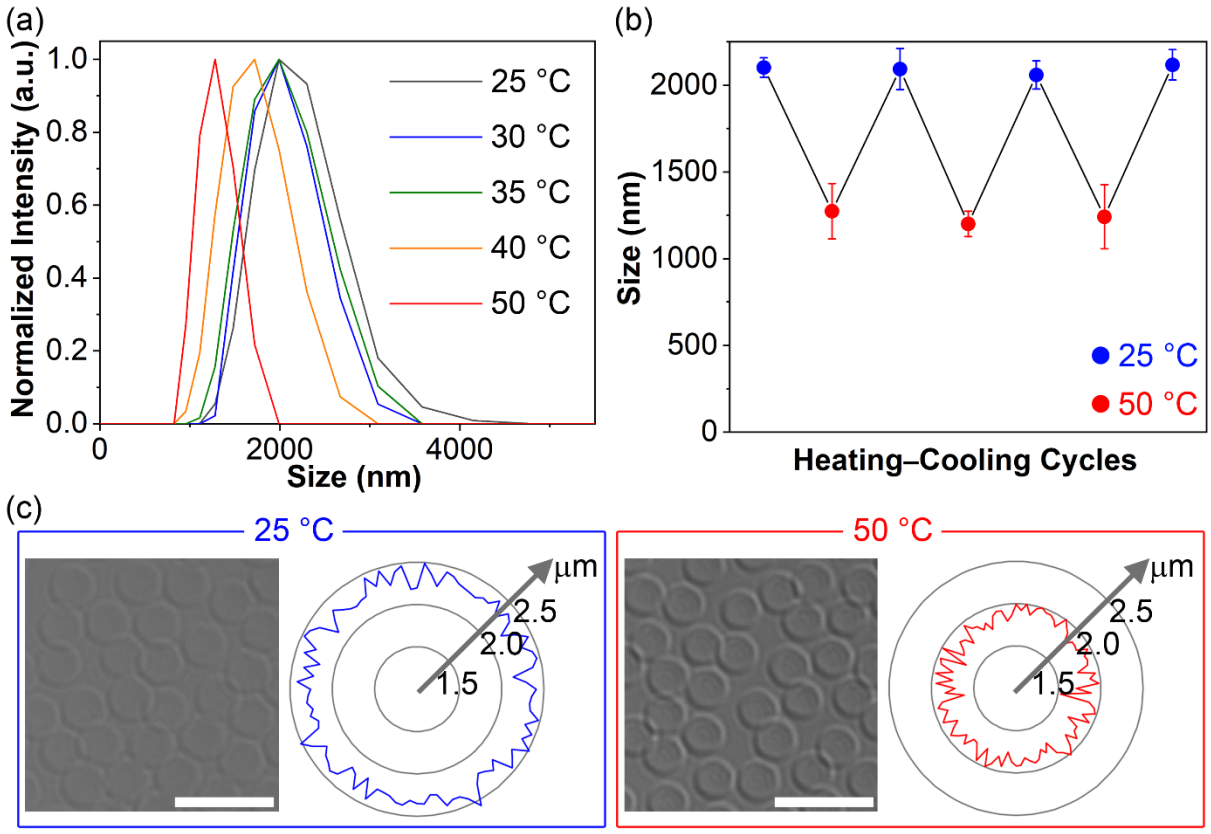

Figure 2. Temperature-induced size reduction of MPN capsules. DLS size measurements of (a) PNIPAM$_{364}$–Fe^{III} MPN capsules at different temperatures and (b) PNIPAM$_{364}$–Fe^{III} MPN capsules when subjected to heating–cooling cycles at 25 and 50 °C. The hydrodynamic diameters, determined by DLS (intensity), are shown as the mean ± standard deviation of three measurements. (c) DIC images and radar maps (from size measurements of 100 capsules) of PNIPAM$_{364}$–Fe^{III} MPN capsules at 25 °C (2.3 ± 0.1 μm) and 50 °C (1.9 ± 0.1 μm). Scale bars are 5 μm.

To further explore the thermoresponsive properties of the MPNs, four different types of PNIPAM$_n$–Fe^{III} MPN capsules were fabricated using PNIPAM$_n$ with different degrees of polymerization (n = 55, 151, 237, and 364), and the resulting capsules were characterized by DIC, SEM, TEM, and AFM (Figure S8). All PNIPAM–Fe^{III} MPN capsules were well dispersed in solution, as observed from the DIC images. In the air-dried state, all capsules featured typical surface morphologies (i.e., folds and creases), as observed from the SEM, TEM, and AFM images. When the temperature was increased from 25 to 50 °C, the size of the PNIPAM–Fe^{III} MPN capsules reduced to differing extents, depending

on the degree of polymerization of PNIPAM (Figures 3a and S9). Specifically, increasing the chain length from biscatechol-PNIPAM$_{55}$ to biscatechol-PNIPAM$_{364}$ led to an increasing degree of thermally induced capsule size contraction—a reduction in size of 2.7%, 16.3%, 32.4%, and 40.3% was observed for PNIPAM$_{55}$, PNIPAM$_{151}$, PNIPAM$_{237}$, and PNIPAM$_{364}$, respectively, when the temperature was increased from 25 to 50 °C. The shell thickness of the PNIPAM–Fe^{III} MPN capsules varied according to the PNIPAM chain length, with the thickness ranging from 10.9 to 13.9 nm (Figure 3b). This thickness range is comparable to the shell thickness of TA–Fe^{III} MPN capsules (10 nm).[30] When the temperature was increased from 25 to 50 °C, the shell thickness of PNIPAM$_{237}$–Fe^{III} and PNIPAM$_{364}$–Fe^{III} MPN capsules increased from 12.7 to 14.3 nm and from 13.9 to 16.1 nm, respectively. In contrast, the shell thickness of the PNIPAM$_{55}$–Fe^{III} and PNIPAM$_{151}$–Fe^{III} capsules, which include shorter PNIPAM chains, remained unchanged upon heating. This is likely due to their higher density of cross-links and therefore more rigid shell structures (Figure 3b).

To further elucidate the tunability of the system, the effect of PNIPAM concentration in the assembly solution on the temperature-dependent contraction of the capsules was examined while the catechol-to-Fe^{III} ion molar ratio was maintained at 1:1. As observed from Figure S10a, the thermoresponsiveness of the MPN capsules prepared with 0.25, 0.5, and 1 mM PNIPAM$_{364}$ could be tuned, as determined from the reduction in capsule size in response to a temperature increase. Specifically, when the temperature was increased from 25 to 50 °C, MPN capsules assembled from 0.25, 0.5, and 1 mM PNIPAM$_{364}$ decreased in size by 1.6%, 40.3%, and 51.3%, respectively. This effect is likely due to the higher amount of PNIPAM building blocks in the capsules. Therefore, increasing the concentration of PNIPAM in the assembly solution can be used to enhance the temperature-dependent size change of the resulting capsules.

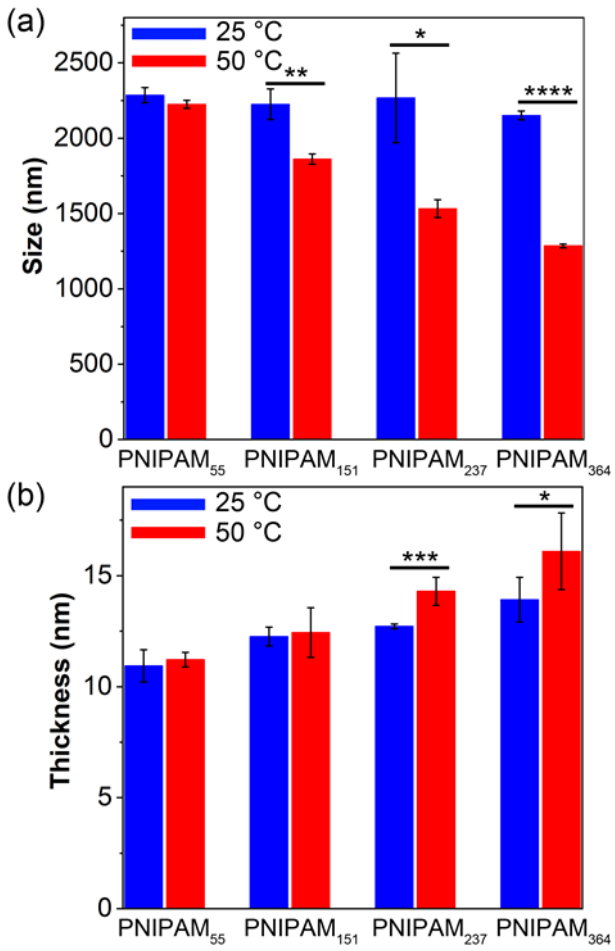

Figure 3. (a) Effect of PNIPAM length on the thermoresponsive properties of PNIPAM$_n$–Fe^{III} MPN capsules (n = 55, 151, 237, and 364). The hydrodynamic diameters, determined by DLS (intensity) at 25 and 50 °C, are shown as the mean ± standard deviation of three independent measurements. (b) Shell thickness of PNIPAM$_n$–Fe^{III} MPN capsules (n = 55, 151, 237, and 364) at different temperatures. The shell thickness was determined by height–distance AFM analysis and is shown as the mean ± standard deviation of five independent AFM measurements. Statistical significance was determined by one-way ANOVA analysis: **** $p < 0.0001$, *** $p < 0.001$, ** $p < 0.01$, and * $p < 0.05$.

The effect of varying the molar ratio of catechol-to-Fe^{III} ions during film assembly was investigated while maintaining the concentration of PNIPAM in the assembly solution at 0.5 mM. As observed from Figure S10b, increasing the catechol-to-Fe^{III} ion molar ratio from 1:0.5 to 1:2 led to MPN capsules with a lower degree of thermoresponsiveness. Specifically, at a catechol-to-Fe^{III} ion molar ratio of 1:0.5, when the temperature was increased to 50 °C, the capsules contracted to 82.9% of their

original diameter at 25 °C. The polydispersity index (PDI) values at 35, 40, and 50 °C increased considerably to 0.49, 0.64, and 0.86, respectively, indicating that the stability of the capsules was reduced. All other prepared PNIPAM$_n$–Fe^{III} capsules were well dispersed at 25–50 °C (PDI < 0.20). In contrast at a catechol-to-Fe^{III} ion molar ratio of 1:2, the capsule size contraction was minimal (12.1%) when the temperature increased from 25 to 50 °C. These results demonstrate that thermoresponsive MPN capsules can be fabricated via MPN chemistry between biscatechol-PNIPAM and Fe^{III} ions, and that the length and concentration of the PNIPAM in the assembly solution and the catechol-to-metal ion molar ratio can be used to effectively tune the thermally induced contraction of MPN capsules.

Effect of Metal Ions on MPN Capsule Thermoresponsive Properties. The physicochemical and functional properties of MPN films can be manipulated by the choice of the metal ions used in the assembly.[36,38,46] For example, the metal ions can be used to impart imaging functionality (e.g., fluorescence imaging, magnetic resonance imaging, and positron emission tomography imaging),[36] facilitate disassembly over a physiologically relevant pH range,[36] control film permeability,[38] or enhance association toward antigens.[46] We hypothesized that the selection of metal ion would influence the thermoresponsive properties of the PNIPAM–metal ion MPN capsules. To verify this hypothesis, biscatechol-PNIPAM$_{364}$ was employed to prepare MPN capsules via coordination with 17 different metal ions: Al^{III}, V^{III}, Cr^{III}, Mn^{II}, Co^{II}, Ni^{II}, Cu^{II}, Zn^{II}, Zr^{IV}, Mo^{II}, Rh^{III}, Ag^{I}, Cd^{II}, Ce^{III}, Eu^{III}, Gd^{III}, and Tb^{III}. The resulting capsules were characterized by SEM, TEM, HAADF, EDX elemental mapping, and AFM. Typical collapsed capsule structures (in the air-dried state) were observed for each metal ion examined (Figures 4a, S11–S14). Moreover, EDX elemental mapping revealed that the respective metal ions were distributed throughout the MPN capsules, which is consistent with the HAADF results (Figures 4a and S13). The data revealed that the MPN capsule size and shell thickness both varied according to the type of the metal ion used. The size of the MPN capsules, in the air-dried state, ranged from 1.3 to 2.0 μm despite using the same template particles (PS-COOH, 1.86 μm)

(Figure S11b). The PNIPAM$_{364}$–V^{III}, PNIPAM$_{364}$–Mn^{II}, PNIPAM$_{364}$–Co^{II}, PNIPAM$_{364}$–Ni^{II}, and PNIPAM$_{364}$–Mo^{II} MPN capsules ranged from 1.3 to 1.4 μm and were smaller than the MPN capsules prepared using other metal ions (capsule size ranged from 1.7 to 2.0 μm). These capsule size differences are likely due to the differing stability constants between the catechol and the specific metal ion (Table S2). Specifically, Mn^{II} and Co^{II} have lower binding affinities to catechol compared with Al^{III} and Fe^{III}, and thus PNIPAM$_{364}$–Mn^{II} and PNIPAM$_{364}$–Co^{II} capsules shrank to 1.3 ± 0.1 and 1.4 ± 0.1 μm, respectively, after template particle removal due to the lower cross-linking density of the network.[38] Generally, the PNIPAM$_{364}$–metal ion MPN capsules exhibited a shell thickness ranging from 6.0 to 16.7 nm, which is comparable to the shell thickness of TA–Fe^{III} capsules (10 nm) (Figure S14b). However, PNIPAM$_{364}$–V^{III}, PNIPAM$_{364}$–Mn^{II}, PNIPAM$_{364}$–Co^{II}, and PNIPAM$_{364}$–Ni^{II} MPN capsules exhibited thicker shells, with thicknesses of 32.8, 21.7, 22.8, and 23.1 nm, respectively. These data show that the selection of the metal ions can be used to tune the size and shell thicknesses of MPN capsules formed using biscatechol-PNIPAM.

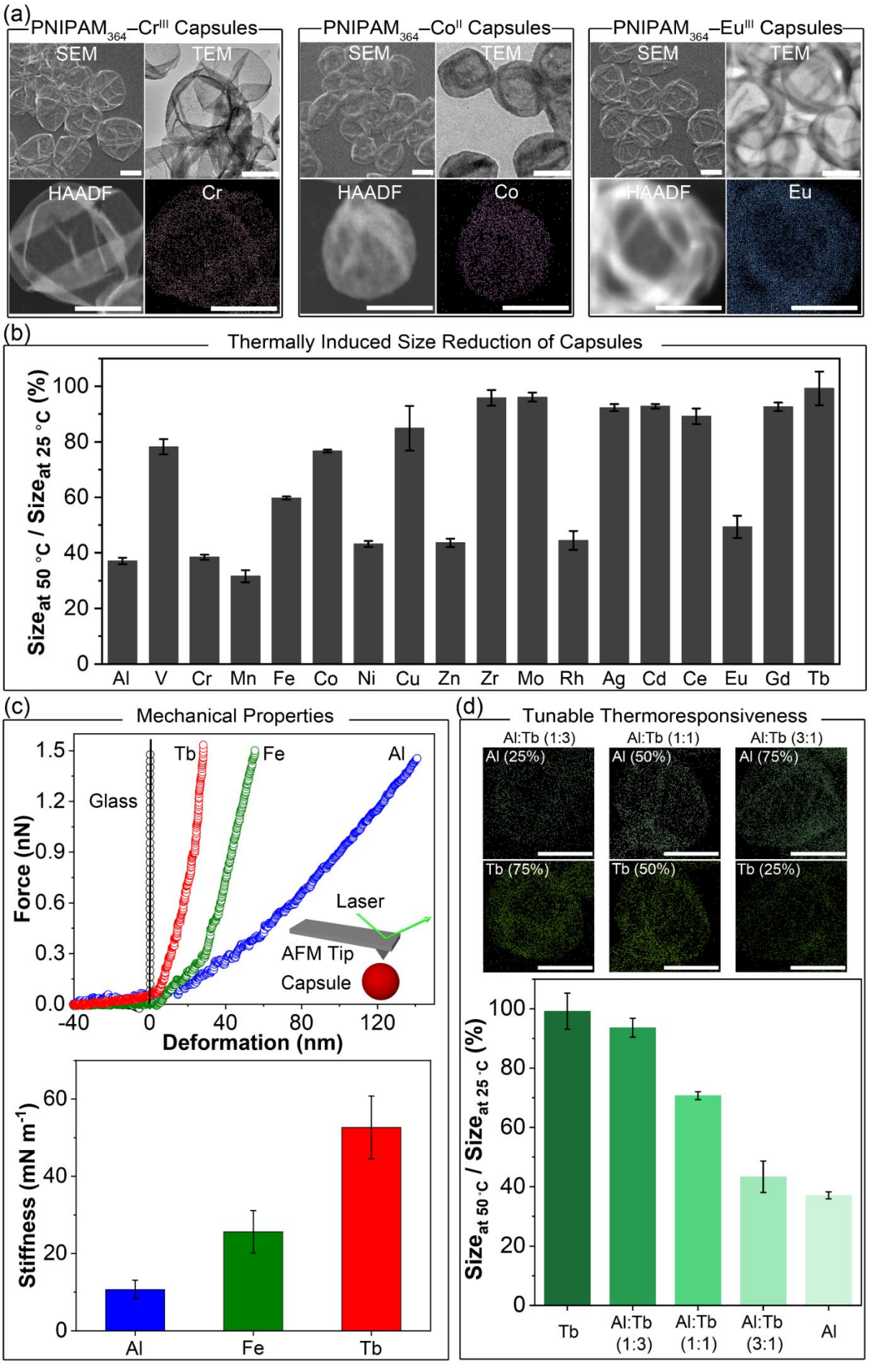
(a)
PNIPAM364–CrIII Capsules
PNIPAM364–CoII Capsules
PNIPAM364–EuIII Capsules
SEM
TEM
HAADF
Cr
Co
Eu
(b)
Thermally Induced Size Reduction of Capsules
Size at 50 °C / Size at 25 °C (%)
Al V Cr Mn Fe Co Ni Cu Zn Zr Mo Rh Ag Cd Ce Eu Gd Tb
(c)
Mechanical Properties
Force (nN)
Deformation (nm)
Glass
Tb
Fe
Al
Laser
AFM Tip
Capsule
Stiffness (mN m-1)
Al Fe Tb
(d)
Tunable Thermoresponsiveness
Al:Tb (1:3)
Al:Tb (1:1)
Al:Tb (3:1)
Al (25%)
Al (50%)
Al (75%)
Tb (75%)
Tb (50%)
Tb (25%)
Size at 50 °C / Size at 25 °C (%)
Tb
Al:Tb (1:3)
Al:Tb (1:1)
Al:Tb (3:1)
Al

Figure 4. Thermoresponsive MPN capsules assembled with various metal ions. (a) SEM, TEM, HAADF, and EDX elemental mapping of PNIPAM$_{364}$–Cr^{III}, PNIPAM$_{364}$–Co^{II}, and PNIPAM$_{364}$–Eu^{III} MPN capsules. Scale bars are 1 μm. (b) Size reduction of PNIPAM$_{364}$–metal ion MPN capsules from 25 to 50 °C, as determined from DLS. (c) Representative force–deformation (F–δ) curves and corresponding stiffness profiles of the PNIPAM$_{364}$–Al^{III}, PNIPAM$_{364}$–Fe^{III}, and PNIPAM$_{364}$–Tb^{III} MPN capsules. The F–δ curve of a glass substrate is also shown for comparison. The data are shown as mean stiffness ± standard deviation (n = 5). (d) EDX elemental mapping of dual metal MPN capsules with varying Al and Tb ratios (1:3, 1:1, and 3:1) (scale bars are 1 μm) and corresponding size reduction profiles from 25 to 50 °C of the PNIPAM$_{364}$–Tb^{III}, PNIPAM$_{364}$–Al^{III}, and PNIPAM$_{364}$–Al^{III}/Tb^{III} MPN capsules. The hydrodynamic diameters, determined by DLS (intensity) at 25 and 50 °C, are shown as the mean ± standard deviation of three independent measurements.

The temperature-triggered contraction of the thermoresponsive MPN capsules prepared from various metal ions was examined by DLS at temperatures below and above the LCST (i.e., 25 and 50 °C) (Figure 4b). Although all capsules were prepared using the same procedures and conditions (i.e., MPN film deposition onto the surface of the PS-COOH template particles, followed by template removal using THF, and the same biscatechol-PNIPAM and identical concentrations of the building blocks), the temperature-triggered size reduction of the capsules differed depending on the metal ion used in the assembly. For example, when the temperature was increased above the LCST, the sizes of the PNIPAM$_{364}$–Al^{III}, PNIPAM$_{364}$–Cr^{III}, and PNIPAM$_{364}$–Mn^{II} capsules were 37.1, 38.4, and 31.6%, respectively, of the corresponding original capsule sizes at 25 °C (which represent size reductions of 62.9%, 61.6%, and 68.4% respectively) (Figure 4b). In contrast, the size of the PNIPAM$_{364}$–Zr^{IV}, PNIPAM$_{364}$–Mo^{II}, and PNIPAM$_{364}$–Tb^{III} MPN capsules decreased by only 1.4%, 5.3%, and 0.9%, respectively (Figure 4b).

The force–deformation (F–δ) curves of the PNIPAM$_{364}$–Al^{III}, PNIPAM$_{364}$–Fe^{III}, and PNIPAM$_{364}$–Tb^{III} capsules, which showed high, moderate, and low temperature-induced contraction, were

examined by AFM force measurement analysis (Figure 4c). The stiffness values, determined from the slope of the curves,[32,47] were 10.7 ± 2.2, 25.6 ± 4.9, and 52.6 ± 7.3 mN m^{-1} for the $PNIPAM_{364}$–Al^{III}, $PNIPAM_{364}$–Fe^{III}, and $PNIPAM_{364}$–Tb^{III} MPN capsules, respectively. The stiffness of the capsules increased with decreasing thermoresponsiveness of the capsules, indicating that a rigid capsule shell results in a low degree of temperature-triggered contraction of the thermoresponsive MPN capsules. The stiffness values of the other $PNIPAM_{364}$–metal ion MPN capsules, i.e., $PNIPAM_{364}$–Cu^{II}, $PNIPAM_{364}$–Zn^{II}, $PNIPAM_{364}$–Mo^{II}, and $PNIPAM_{364}$–Ce^{III}, were determined to be 32.3 ± 4.3, 12.9 ± 1.0, 53.8 ± 5.6, and 43.9 ± 5.5 mN m^{-1}, and followed the same mechanical property–thermoresponsive behavior trend (Figure S15—increasing stiffness resulted in less thermoresponsive capsules that displayed a smaller size contraction as the temperature increased from 25 to 50 °C).

We hypothesized that the temperature-dependent size reduction of the PNIPAM–metal ion MPN capsules could be further tuned by incorporating two different metal ions during MPN assembly (Figure 4d). To illustrate this, Al and Tb were selected as the metal ions as $PNIPAM_{364}$–Al^{III} and $PNIPAM_{364}$–Tb^{III} capsules showed contrasting levels of contraction upon heating (i.e., 63.9 % vs 0.9 %). The effect of varying the molar ratio of Al and Tb (1:3, 1:1, and 3:1) while maintaining a constant total metal ion concentration was examined. As anticipated, increasing the proportion of Al in the $PNIPAM_{364}$–Al^{III}/Tb^{III} MPN capsules resulted in a greater thermally induced reduction in size of the capsules. These results indicate that the thermoresponsive properties of the PNIPAM–metal ion MPN capsules are controllable through both the specific choice of metal ion and employing binary mixtures of suitably chosen metal ions.

MPN Capsule Temperature-Dependent Permeability Control and Cargo Encapsulation/Release. The permeability of the $PNIPAM_n$–Fe^{III} MPN capsules (n = 55, 151, 237, and 364) was examined by incubating the capsules with FITC-dextran with molecular weights ranging from 4 to 2000 kDa. The Stokes radius of the FITC-dextran molecules varies according to their molecular weight, where higher molecular weight FITC-dextran molecules have a larger size.[48,49]

Generally, the permeability of the PNIPAM$_n$–Fe^{III} MPN capsules was higher than that of TA–Fe^{III} MPN capsules. Specifically, more than 90% of PNIPAM$_n$–Fe^{III} MPN capsules (Figure S16) and 38.0% of TA–Fe^{III} MPN capsules[30] were permeable to 68 kDa FITC-dextran. This higher permeability of the PNIPAM$_n$–Fe^{III} MPN capsules is likely due to their less dense network structure and the fewer number of anchor points in biscatechol-PNIPAM (vs TA) when compared with that of the TA–Fe^{III} MPN capsules. As the permeability of MPN capsules can be regulated through the choice of phenolic building blocks,[38] we hypothesized that the PNIPAM$_n$–Fe^{III} MPN capsules prepared with PNIPAM of variable chain length would show different permeabilities. As validated in Figure S16, increasing the chain length of the PNIPAM building blocks increased the permeability of the capsules. Specifically, 23.7% of PNIPAM$_{55}$–Fe^{III} MPN capsules, 64.6% of PNIPAM$_{151}$–Fe^{III} MPN capsules, 75.0% of PNIPAM$_{237}$–Fe^{III} MPN capsules, and 88.6% of PNIPAM$_{364}$–Fe^{III} MPN capsules were permeable to 500 kDa FITC-dextran.

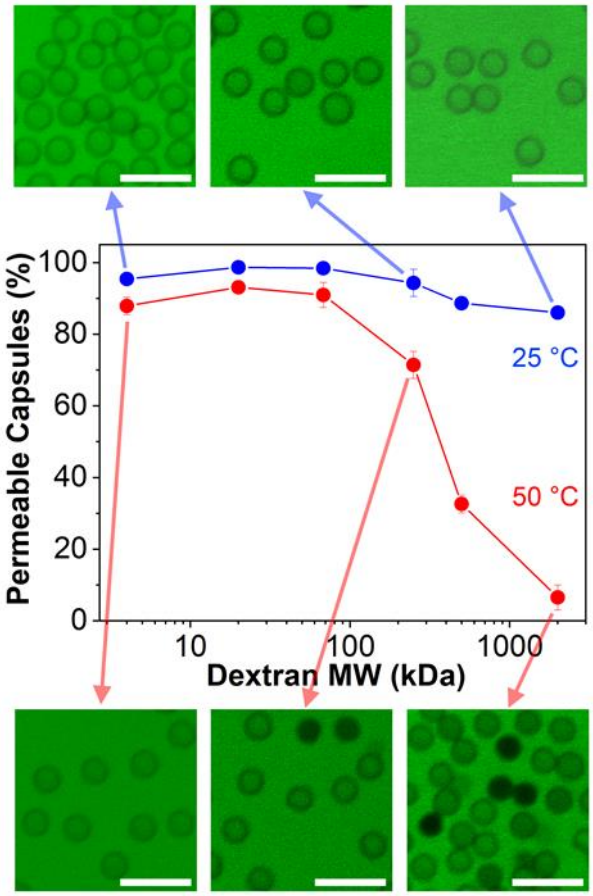

Figure 5. Temperature-dependent permeability of PNIPAM$_{364}$–Fe^{III} MPN capsules to FITC-dextran with molecular weight (MW) from 4 to 2000 kDa and corresponding representative confocal microscopy images (scale bars are 5 μm). The permeability data are shown as the mean ± standard deviation of three independent experiments; 100–150 capsules were examined.

The PNIPAM$_{364}$–Fe^{III} MPN capsules were investigated further to assess whether their permeability could be additionally tuned with changes in the temperature. Such a behavior might be applicable in diverse fields such as nano/microreactors, separations, sensing, and therapeutic delivery.[2,7–9,50] As observed from Figures 5 and S17, the permeability of the thermoresponsive capsules decreased when the temperature was increased from 25 to 50 °C. Specifically, 88.6% and 86.0% of the capsules were permeable to 500 and 2000 kDa FITC-dextran, respectively, at 25 °C. However, when the temperature was increased to 50 °C, the permeability decreased to 32.6% and 6.5%, respectively. These results indicate a reduction in pore size upon increasing the temperature in addition to the previously discussed reduction in capsule diameter. The capsule permeability as a function of temperature was also investigated using PNIPAM$_{364}$-based MPN capsules prepared with metal ions other than Fe^{III} ions. As observed from Figures S18 and S19, PNIPAM$_{364}$–Al^{III} MPN capsules, which showed a large thermoresponsive size contraction (~63%, Figure 4b), exhibited thermally induced permeability changes to a similar extent to the changes observed for PNIPAM$_{364}$–Fe^{III} MPN capsules. In contrast, PNIPAM$_{364}$–Tb^{III} MPN capsules, which showed minimal thermally induced size contraction (~1%, Figure 4b), did not show a significant change in permeability with changes in the temperature (Figures S18 and S20).

The tunable temperature-dependent permeability displayed by the thermoresponsive MPN capsules can be used to facilitate dynamic cargo encapsulation and release. To demonstrate this, PNIPAM$_{364}$–Fe^{III} MPN capsules were incubated with 500 kDa FITC-dextran at 25 °C; under these conditions, the cargo can freely diffuse into the capsules (Figure 6a, permeable state). The 500 kDa FITC-dextran was then encapsulated within the capsules by increasing the temperature above the LCST, which converted

the shell into an impermeable state, and subsequent washing with MOPS buffer at 50 °C. The capsules exhibited bright green fluorescence, as observed by confocal laser scanning microscopy (CLSM) (Figure 6a, encapsulation). The observed annular fluorescence of the capsules likely originates from hydrogen bonding interactions between dextran and the PNIPAM film, leading to localization of the dextran in/on the capsule wall, which is consistent with previous observations.[51] In contrast, when the capsules were loaded with 500 kDa FITC-dextran and subsequently washed with MOPS buffer at a temperature below the LCST, a considerably lower loading efficiency was observed (i.e., a loading efficiency of 17% was obtained, which was lower than the loading efficiency obtained when encapsulation was performed at 50 °C). The faint fluorescence is likely derived from hydrogen bonding between the cargo molecules and the MPN film (Figure S21). When the temperature of the capsules loaded with 500 kDa FITC-dextran was decreased to below the LCST, the encapsulated 500 kDa FITC-dextran was released, indicating that under these conditions the MPN film reverts to a permeable state (Figure 6a, release). The kinetics of cargo release from $PNIPAM_{364}$–Fe^{III} MPN capsules was investigated over time at 25 °C (Figure 6b). Specifically, the release of 500 kDa FITC-dextran (%) was evaluated as the ratio of the mean fluorescence intensity detected outside the capsules to that at the rim of capsules. The 500 kDa FITC-dextran cargo was continually released, reaching approximately 70% after 90 min. These results demonstrate the potential to apply thermoresponsive MPN capsules with temperature-dependent permeability for encapsulation and release applications. Importantly, while the present system exhibits higher permeability at lower temperatures (i.e., below the LCST), it is envisaged that substituting PNIPAM with a polymer having a UCST may result in the opposite behavior: higher permeability at elevated temperature and lower permeability at lower temperatures. Nevertheless, the present study represents proof-of-principle that thermoresponsive polymers can be employed in the fabrication of MPN capsules and highlights the importance of ongoing research and development in this area to prepare bespoke materials suitable for specific applications. Furthermore, $PNIPAM_{364}$–metal ion MPN capsules showed negligible cytotoxicity,

suggesting their potential for biomedical and environmental applications (Figure S22). We note, however, that PNIPAM$_{364}$–Mn^{II} and PNIPAM$_{364}$–Cd^{II} MPN capsules showed some cytotoxicity to cells, likely due to the toxicity of the metal ion employed in the specific structure.[52,53] Moreover, such micrometer-sized capsules have potential use in vaccine and pulmonary delivery.[32,54–57]

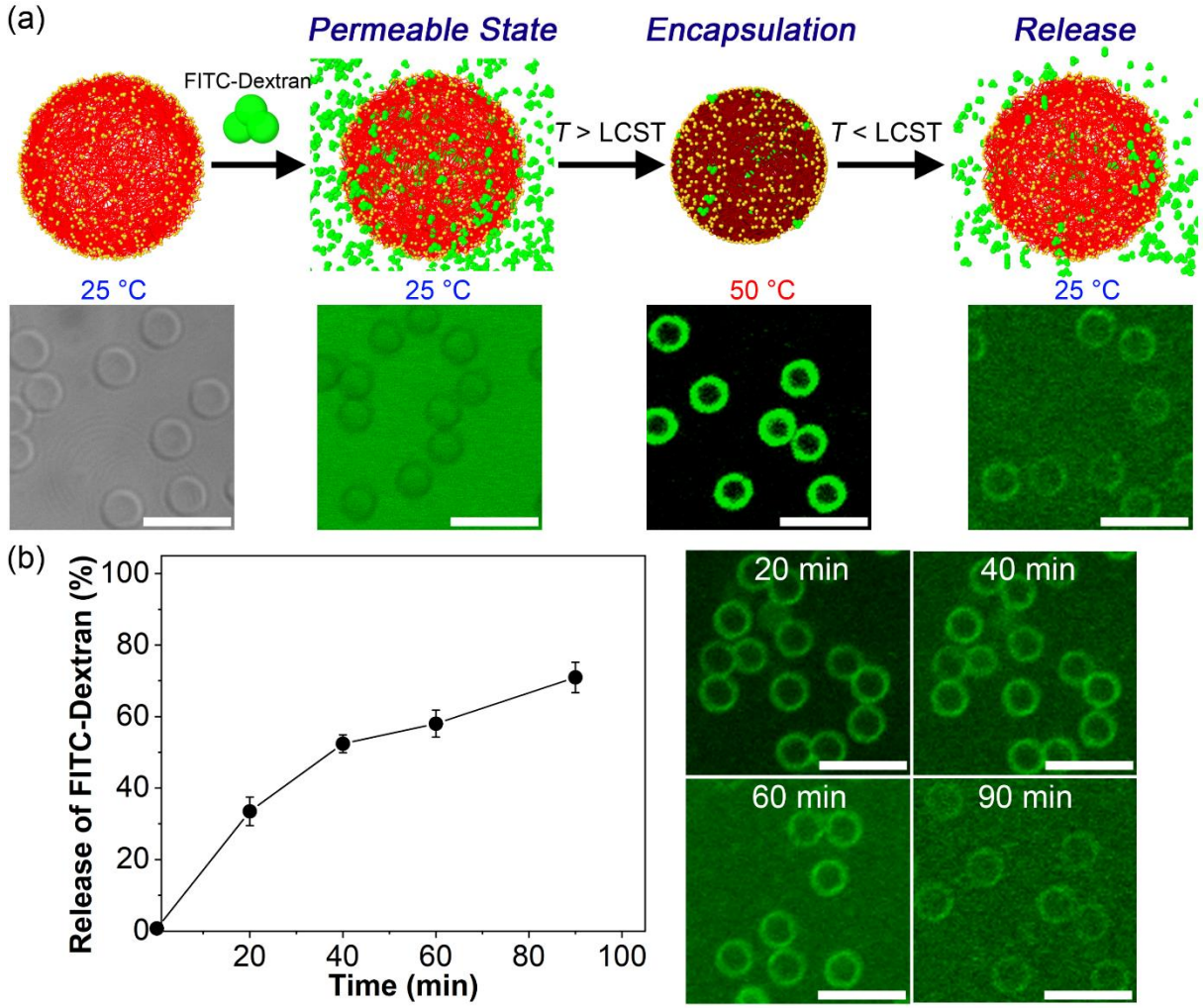

Figure 6. (a) Schematic and corresponding CLSM images of thermally induced encapsulation and release of FITC-dextran (500 kDa) from thermoresponsive PNIPAM$_{364}$–Fe^{III} MPN capsules. (b) Release of FITC-dextran (500 kDa) from capsules over 90 min at 25 °C and associated CLSM images. Scale bars in (a) and (b) are 5 μm.

CONCLUSION

We have described the synthesis of biscatechol-functionalized PNIPAM via RAFT polymerization, and the subsequent fabrication of various PNIPAM$_n$–metal ion MPN capsules. Four different lengths

of biscatechol-PNIPAM chains (n = 55, 151, 237, 364) were synthesized, and the formation of MPN networks with biscatechol-PNIPAM was demonstrated with 18 different metal ions. The resulting MPN capsules exhibited tunable thermally induced size changes, depending on the selection of the building blocks, i.e., biscatechol-PNIPAM and metal ions. $PNIPAM_{364}$–Fe^{III} MPN capsules showed the largest size reduction when the temperature was increased above the LCST among the $PNIPAM_n$–Fe^{III} MPN capsules assembled from different PNIPAM chain lengths. These results indicate that the chain length of PNIPAM influences the thermoresponsive properties of the capsules formed. The temperature-induced size change behavior displayed by the capsules was reversible and was associated with an increase in the shell thickness of the capsules. Variation of the metal ion used in the assembly led to differing extents of temperature-induced size contraction (1–68% upon heating from 25 to 50 °C), providing an alternative approach by which the thermoresponsive properties of the capsules can be tuned. These different thermoresponsive properties were associated with the mechanical properties of the capsules: more rigid capsules showed reduced temperature-triggered capsule size contraction when compared with less rigid capsules. The thermoresponsive properties of the capsules could also be tuned by controlling the ratio of a binary mixture of two different metal ions (e.g., Al and Tb). Temperature-dependent size changes of the MPN capsules also affected the shell permeability, as demonstrated from the loading and release of FITC-dextran with various molecular weights. $PNIPAM_{364}$–Fe^{III} MPN capsules showed higher permeability to 4–2000 kDa FITC-dextran at room temperature than TA–Fe^{III} MPN capsules, likely due to the lower number of anchor sites on biscatechol-PNIPAM compared to TA. Above the LCST, a considerable decrease in the permeability of the capsules to higher molecular weights of FITC-dextran was observed, due to the denser network structure formation of the capsules. The temperature-responsive permeability change of the capsules was exploited to encapsulate and release cargo in response to temperature changes. Collectively, the findings can provide a platform for the rational design of thermoresponsive capsules using other more biocompatible polymers (e.g., poly(*N*-vinyl caprolactam)[58] or polymers having UCST character (e.g.,

poly(acrylonitrile-*co*-acrylamide)[59]) facilitating cargo encapsulation at a lower temperature (e.g., 25 °C) and release at a higher temperature (e.g., 37 °C). The development of thermoresponsive MPN capsules is an important step in the fabrication of dynamic nanostructured materials for potential applications in various fields.

EXPERIMENTAL SECTION

Synthesis of PNIPAM–Metal Ion MPN Capsules. The PNIPAM–Fe^{III} MPN capsules were prepared as follows. A PS-COOH (1.86 ± 0.03 μm, 100 mg mL^{-1}) particle dispersion (50 μL) was transferred to a 1.7 mL microcentrifuge tube and washed twice with water. The PS-COOH particles were washed with water by vortexing and sonication for 1–2 min and then pelleted by centrifugation (2000 *g*, 2 min). The supernatant was then discarded, and the process was repeated. A biscatechol-PNIPAM stock solution and $FeCl_3 \cdot 6H_2O$ solution were added to the particle suspension to obtain final concentrations of 0.5 and 1 mM, respectively, and mixed by vortexing for 2 min. The final concentration of the PS-COOH particles was 10 mg mL^{-1}. MOPS buffer (25 mM, pH 7.4, 0.7 mL) was then added to raise the pH above 7, leading to the formation of bis- and tris-coordination complexes between biscatechol-PNIPAM and Fe^{III} ions. After increasing the pH, excess and unreacted materials were removed by pelleting the particles (2000 *g*, 2 min) and the supernatant was discarded. The MPN-coated particles were washed three times with water (500 μL) by repeated centrifugation (2000 *g*, 2 min) and redispersion. The particles were then resuspended in water (50 μL), and THF (1 mL) was added to remove the template particles. After 1 h, the MPN capsules were pelleted through centrifugation (2000 *g*, 2 min) and washed with THF (500 μL) five times. At the final THF washing step, the capsules were pelleted through centrifugation (2000 *g*, 3 min) and the supernatant was discarded. The resulting PNIPAM–Fe^{III} MPN capsules were washed with water once and resuspended in water (300 μL).

PNIPAM$_{364}$–metal ion MPN capsules composed of different metal ions Al, V, Cr, Mn, Co, Ni, Cu, Zn, Zr, Mo, Rh, Ag, Cd, Ce, Eu, Gd, or Tb and PNIPAM$_{364}$–Al^{III}/Tb^{III} (1:3, 1:1, and 3:1) MPN capsules were prepared using the same preparation method as that used for the PNIPAM–Fe^{III} MPN capsules.

Preparation of Amine-Terminated Glass Substrates. Glass substrates were functionalized with 3-(aminopropyl)triethoxysilane (APTES). For the functionalization, a 0.5% APTES solution was first prepared by dissolving APTES (400 μL) in ethanol (80 mL). The glass substrates were then immersed in 0.5% APTES solution for 24 h, followed by thorough rinsing with ethanol and water. The obtained amine-functionalized glass substrates were stored in water and dried under a stream of air before use.

Temperature-Dependent Size Changes of Thermoresponsive MPN Capsules. Various analyses were performed to characterize the temperature-dependent size changes of the thermoresponsive capsules. For DLS analysis, the PNIPAM–metal ion MPN capsules were first dispersed in water. The thermally induced size changes of the capsules were monitored at 25–50 °C with 10 min equilibration time at each temperature. For DIC microscopy analysis, a fresh MPN-coated PS-COOH suspension (100 μL) was dropped onto an amine-terminated glass substrate and left undisturbed for 2 h. The glass substrate was then immersed in fresh THF for 2 h to remove the template particles. The remaining THF was removed by immersing the coated substrates twice in water. Water (200 μL) was then added to the capsule area on the glass substrate at 25 °C and the DIC microscopy images were recorded. To collect the DIC images at temperatures above LCST, the capsule area on the glass substrates was immersed in hot water (50 °C) for 30 min and the temperature control stage of the microscope was set to 50 °C. Hot water (50 °C, 200 μL) was then added to the capsule area on the glass substrate and the DIC images were recorded.

Mechanical Studies. A fresh MPN-coated PS-COOH suspension (30 μL) was dropped onto a sectioned amine-terminated glass substrate (1 cm × 1 cm) and left undisturbed for 2 h. Then, the capsules were prepared onto the glass substrate using THF and water treatment following the same protocol for the DIC and confocal microscopy analyses. The measurements were performed on a

Cypher atomic force microscope (Asylum Research, Goleta, CA, USA) in ultrapure water (18.2 MΩ cm) with BioLever mini cantilevers (spring constant 0.02–0.14 N m^{-1}, Olympus, Tokyo, Japan). The spring constant of the cantilever was determined to be 0.062 N m^{-1}. The location of individual capsules was identified through AFM imaging under tapping mode. An individual capsule was then indented with the AFM tip at a specified applied force (1.5 nN) and a constant velocity (0.5 μm s^{-1}) under contact mode, and the resulting $F–\delta$ curve was recorded. The $F–\delta$ curves of five different capsules were collected and analyzed using Asylum Research software.

Temperature-Dependent Permeable Properties of Thermoresponsive MPN Capsules. To assess the permeability of the MPN capsules, the capsules were prepared using the same procedure as used for DIC analysis. A fresh MPN-coated PS-COOH suspension (100 μL) was dropped onto an amine-terminated glass substrate and left undisturbed for 2 h. The glass substrate was then immersed in fresh THF for 2 h to remove the template particles. The remaining THF was removed by immersing twice in water. An FITC-dextran solution (200 μL, 1 mg mL^{-1}) was then added to the capsule area on the glass substrate. After 5 min, CLSM images of the capsules were taken at 25 °C. To determine the permeability at 50 °C, the capsule area on the glass substrates and the FITC-dextran solution (1 mg mL^{-1}) were kept in hot water (50 °C) for 30 min and the temperature control stage of the microscope was set to 50 °C. The FITC-dextran solution (200 μL, 1 mg mL^{-1}, 50 °C) was then added to the capsule area on the glass substrate. After 5 min, CLSM images of the capsules were taken at 50 °C. Dark capsule interiors were considered to indicate the formation of an impermeable film, whereas capsules with interiors of fluorescence intensity similar to the outer environment were considered to be permeable. Approximately 100–150 capsules were examined. The permeability of the capsules is reported as the percentage of permeable capsules.

Cargo Encapsulation and Release Studies. To load cargo molecules into the capsules, 500 kDa FITC-dextran (200 μL, 5 mg mL^{-1} in 25 mM MOPS) was added to an area containing the $PNIPAM_{364}$–Fe^{III} capsules on a glass substrate. After 5 min of incubation, FITC-dextran (200 μL), which was kept

at 50 °C for 30 min, was added to the capsule area and the temperature control stage of the microscope was increased to 50 °C to entrap FITC-dextran molecules inside the capsules. After 30 min, the FITC-dextran solution was replaced with MOPS buffer solution (1000 µL, 25 mM) at 50 °C. To release the cargo molecules, hot MOPS buffer (1000 µL, 25 mM, 50 °C) on the glass substrate was replaced with MOPS (400 µL, 25 mM, 25 °C) at 25 °C, and the temperature control stage of the microscope was decreased to 25 °C. The capsules were imaged by confocal microscopy after the desired period of time. The percentage of cargo release was calculated as the ratio of the mean fluorescence intensity measured outside the capsules to that at the rim of the capsules. The data are given as the mean value ± standard deviation.

ASSOCIATED CONTENT

Supporting Information. Materials and instrumentation; synthesis of biscatechol-BCMT; synthesis of biscatechol-PNIPAM; HPLC, NMR, GPC, UV–vis spectroscopy, DIC, SEM, TEM, AFM data, temperature-induced size reduction, and permeability data; and FITC-dextran encapsulation efficiency at 25 °C; and cytotoxicity data.

AUTHOR INFORMATION

Corresponding Author

*E-mail: fcaruso@unimelb.edu.au (F.C.); john.f.quinn@monash.edu (J.F.Q.)

Notes

The authors declare no competing financial interest.

ACKNOWLEDGMENTS

This research was funded by the Australian Research Council (ARC) through the Discovery Project (DP200100713) scheme. F.C. acknowledges the award of a National Health and Medical Research Council Senior Principal Research Fellowship (GNT1135806). J.F.Q. acknowledges receipt of a Future Fellowship (FT170100144) from the ARC. This work was performed in part at the Materials

Characterisation and Fabrication Platform (MCFP) at The University of Melbourne and the Victorian Node of the Australian National Fabrication Facility (ANFF).

REFERENCES

1. Lu, Y.; Aimetti, A. A.; Langer, R.; Gu, Z. Bioresponsive Materials. *Nat. Rev. Mater.* **2016**, *2*, 16075.

2. Mura, S.; Nicolas, J.; Couvreur, P. Stimuli-Responsive Nanocarriers for Drug Delivery. *Nat Mater*. **2013**, *12*, 991–1003.

3. Chan, L. W.; Anahtar, M. N.; Ong, T. H.; Hern, K. E.; Kunz, R. R.; Bhatia, S. N. Engineering Synthetic Breath Biomarkers for Respiratory Disease. *Nat. Nanotechnol*. **2020**, *15*, 792–800.

4. Purcell, B. P.; Lobb, D.; Charati, M. B.; Dorsey, S. M.; Wade, R. J.; Zellars, K. N.; Doviak, H.; Pettaway, S.; Logdon, C. B.; Shuman, J. A. Injectable and Bioresponsive Hydrogels for on-Demand Matrix Metalloproteinase Inhibition. *Nat. Mater.* **2014**, *13*, 653–661.

5. Vazquez-Gonzalez, M.; Willner, I. Stimuli-Responsive Biomolecule-Based Hydrogels and Their Applications. *Angew. Chem., Int. Ed.* **2020**, *59*, 15342–15377.

6. Vriezema, D. M.; Comellas Aragonès, M.; Elemans, J. A.; Cornelissen, J. J.; Rowan, A. E.; Nolte, R. J. Self-Assembled Nanoreactors. *Chem. Rev.* **2005**, *105*, 1445–1490.

7. Liu, Z.; Wang, W.; Xie, R.; Ju, X.-J.; Chu, L.-Y. Stimuli-Responsive Smart Gating Membranes. *Chem. Soc. Rev.* **2016**, *45*, 460–475.

8. Chandrawati, R.; Hosta-Rigau, L.; Vanderstraaten, D.; Lokuliyana, S. A.; Stadler, B.; Albericio, F.; Caruso, F. Engineering Advanced Capsosomes: Maximizing the Number of Subcompartments, Cargo Retention, and Temperature-Triggered Reaction. *ACS Nano* **2010**, *4*, 1351–1361.

9. Chandrawati, R.; Odermatt, P. D.; Chong, S. F.; Price, A. D.; Stadler, B.; Caruso, F. Triggered Cargo Release by Encapsulated Enzymatic Catalysis in Capsosomes. *Nano Lett.* **2011**, *11*, 4958–4963.

10. Du, J.-Z.; Du, X.-J.; Mao, C.-Q.; Wang, J. Tailor-Made Dual pH-Sensitive Polymer–Doxorubicin Nanoparticles for Efficient Anticancer Drug Delivery. *J. Am. Chem. Soc.* **2011**, *133*, 17560–17563.

11. Hartgerink, J. D.; Beniash, E.; Stupp, S. I. Self-Assembly and Mineralization of Peptide-Amphiphile Nanofibers. *Science* **2001**, *294*, 1684–1688.

12. Klaikherd, A.; Nagamani, C.; Thayumanavan, S. Multi-Stimuli Sensitive Amphiphilic Block Copolymer Assemblies. *J. Am. Chem. Soc.* **2009**, *131*, 4830–4838.

13. Kim, C.-J.; Park, J.-e.; Hu, X.; Albert, S. K.; Park, S.-J. Peptide-Driven Shape Control of Low-Dimensional DNA Nanostructures. *ACS Nano* **2020**, *14*, 2276–2284.

14. Chien, M. P.; Rush, A. M.; Thompson, M. P.; Gianneschi, N. C. Programmable Shape-Shifting Micelles. *Angew. Chem., Int. Ed.* **2010**, *49*, 5076–5080.

15. Shim, T. S.; Estephan, Z. G.; Qian, Z.; Prosser, J. H.; Lee, S. Y.; Chenoweth, D. M.; Lee, D.; Park, S.-J.; Crocker, J. C. Shape Changing Thin Films Powered by DNA Hybridization. *Nat. Nanotechnol.* **2017**, *12*, 41–47.

16. Kim, C.-J.; Hu, X.; Park, S.-J. Multimodal Shape Transformation of Dual-Responsive DNA Block Copolymers. *J. Am. Chem. Soc.* **2016**, *138*, 14941–14947.

17. Kim, C.-J.; Jeong, E. H.; Lee, H.; Park, S.-J. A Dynamic DNA Nanostructure with Switchable and Size-Selective Molecular Recognition Properties. *Nanoscale* **2019**, *11*, 2501–2509.

18. Yan, H.; Teh, C.; Sreejith, S.; Zhu, L.; Kwok, A.; Fang, W.; Ma, X.; Nguyen, K. T.; Korzh, V.; Zhao, Y. Functional Mesoporous Silica Nanoparticles for Photothermal-Controlled Drug Delivery In Vivo. *Angew. Chem., Int. Ed.* **2012**, *51*, 8373–8377.

19. Wang, W.; Li, S.; Mair, L.; Ahmed, S.; Huang, T. J.; Mallouk, T. E. Acoustic Propulsion of Nanorod Motors inside Living Cells. *Angew. Chem., Int. Ed.* **2014**, *53*, 3201–3204.

20. Hwang, G.; Paula, A. J.; Hunter, E. E.; Liu, Y.; Babeer, A.; Karabucak, B.; Stebe, K.; Kumar, V.; Steager, E.; Koo, H. Catalytic Antimicrobial Robots for Biofilm Eradication. *Sci. Robot.* **2019**, *4*, eaaw2388.

21. Gao, W.; Sattayasamitsathit, S.; Manesh, K. M.; Weihs, D.; Wang, J. Magnetically Powered Flexible Metal Nanowire Motors. *J. Am. Chem. Soc.* **2010**, *132*, 14403–14405.

22. Blum, A. P.; Kammeyer, J. K.; Rush, A. M.; Callmann, C. E.; Hahn, M. E.; Gianneschi, N. C. Stimuli-Responsive Nanomaterials for Biomedical Applications. *J. Am. Chem. Soc.* **2015**, *137*, 2140–2154.

23. Roy, D.; Brooks, W. L.; Sumerlin, B. S. New Directions in Thermoresponsive Polymers. *Chem. Soc. Rev.* **2013**, *42*, 7214–7243.

24. Schild, H. G. Poly(*N*-Isopropylacrylamide): Experiment, Theory and Application. *Prog. Polym. Sci.* **1992**, *17*, 163–249.

25. Jones, S. T.; Walsh-Korb, Z.; Barrow, S. J.; Henderson, S. L.; del Barrio, J.; Scherman, O. A. The Importance of Excess Poly(*N*-Isopropylacrylamide) for the Aggregation of Poly(*N*-Isopropylacrylamide)-Coated Gold Nanoparticles. *ACS Nano* **2016**, *10*, 3158–3165.

26. Appel, E. A.; Del Barrio, J.; Loh, X. J.; Dyson, J.; Scherman, O. A. High Molecular Weight Polyacrylamides by Atom Transfer Radical Polymerization: Enabling Advancements in Water-Based Applications. *J. Polym. Sci., Part A: Polym. Chem.* **2012**, *50*, 181–186.

27. Zhu, M.-Q.; Wang, L.-Q.; Exarhos, G. J.; Li, A. D. Thermosensitive Gold Nanoparticles. *J. Am. Chem. Soc.* **2004**, *126*, 2656–2657.

28. Zhang, K.; Zhu, X.; Jia, F.; Auyeung, E.; Mirkin, C. A. Temperature-Activated Nucleic Acid Nanostructures. *J. Am. Chem. Soc.* **2013**, *135*, 14102–14105.

29. Moughton, A. O.; O'Reilly, R. K. Thermally Induced Micelle to Vesicle Morphology Transition for a Charged Chain End Diblock Copolymer. *Chem. Commun.* **2010**, *46*, 1091–1093.

30. Ejima, H.; Richardson, J. J.; Liang, K.; Best, J. P.; van Koeverden, M. P.; Such, G. K.; Cui, J.; Caruso, F. One-Step Assembly of Coordination Complexes for Versatile Film and Particle Engineering. *Science* **2013**, *341*, 154–157.

31. Guo, J.; Tardy, B. L.; Christofferson, A. J.; Dai, Y.; Richardson, J. J.; Zhu, W.; Hu, M.; Ju, Y.; Cui, J.; Dagastine, R. R.; Yarovsky, I.; Caruso, F. Modular Assembly of Superstructures from Polyphenol-Functionalized Building Blocks. *Nat. Nanotechnol.* **2016**, *11*, 1105–1111.

32. Ju, Y.; Cortez-Jugo, C.; Chen, J.; Wang, T. Y.; Mitchell, A. J.; Tsantikos, E.; Bertleff-Zieschang, N.; Lin, Y. W.; Song, J.; Cheng, Y.; Mettu, S.; Rahim, A. M.; Pan, S.; Yun, G.; Hibbs, M. L.; Yeo, L. Y.; Hagemeyer, C. E.; Caruso, F. Engineering of Nebulized Metal–Phenolic Capsules for Controlled Pulmonary Deposition. *Adv. Sci.* **2020**, *7*, 1902650.

33. Pan, S.; Richardson, J. J.; Christofferson, A. J.; Besford, Q. A.; Zheng, T.; Wood, B. J.; Duan, X.; Jara Fornerod, M. J.; McConville, C. F.; Yarovsky, I.; Guldin, S.; Jiang, L.; Caruso, F. Fluorinated Metal–Organic Coatings with Selective Wettability. *J. Am. Chem. Soc.* **2021**, *143*, 9972–9981.

34. Zhang, Z.; Li, B.; Xie, L.; Sang, W.; Tian, H.; Li, J.; Wang, G.; Dai, Y. Metal–Phenolic Network-Enabled Lactic Acid Consumption Reverses Immunosuppressive Tumor Microenvironment for Sonodynamic Therapy. *ACS Nano* **2021**, *15*, 16934–16945.

35. Zhang, Z.; Sang, W.; Xie, L.; Li, W.; Li, B.; Li, J.; Tian, H.; Yuan, Z.; Zhao, Q.; Dai, Y. Polyphenol-Based Nanomedicine Evokes Immune Activation for Combination Cancer Treatment. *Angew. Chem., Int. Ed.* **2021**, *60*, 1967–1975.

36. Guo, J.; Ping, Y.; Ejima, H.; Alt, K.; Meissner, M.; Richardson, J. J.; Yan, Y.; Peter, K.; Elverfeldt, D. v.; Hagemeyer, C. E.; Caruso, F. Engineering Multifunctional Capsules through the Assembly of Metal-Phenolic Networks. *Angew. Chem., Int. Ed.* **2014**, *53*, 5546–5551.

37. Cherepanov, P. V.; Rahim, M. A.; Bertleff-Zieschang, N.; Sayeed, M. A.; O'Mullane, A. P.; Moulton, S. E.; Caruso, F. Electrochemical Behavior and Redox-Dependent Disassembly of Gallic Acid/Fe^{III} Metal–Phenolic Networks. *ACS Appl. Mater. Interfaces* **2018**, *10*, 5828–5834.

38. Chen, J.; Pan, S.; Zhou, J.; Zhong, Q.-Z.; Qu, Y.; Richardson, J. J.; Caruso, F. Programmable Permeability of Metal–Phenolic Network Microcapsules. *Chem. Mater.* **2020**, *32*, 6975–6982.

39. Lin, G.; Richardson, J. J.; Ahmed, H.; Besford, Q. A.; Christofferson, A. J.; Beyer, S.; Lin, Z.; Rezk, A. R.; Savioli, M.; Zhou, J.; McConville, C. F.; Cortez-Jugo, C.; Yeo, L. Y.; Caruso, F. Programmable Phototaxis of Metal–Phenolic Particle Microswimmers. *Adv. Mater.* **2021**, *33*, 2006177.

40. Pan, S.; Guo, R.; Bertleff-Zieschang, N.; Li, S.; Besford, Q. A.; Zhong, Q.-Z.; Yun, G.; Zhang, Y.; Cavalieri, F.; Ju, Y.; Goudeli, E.; Richardson, J. J.; Caruso, F. Modular Assembly of Host–Guest Metal–Phenolic Networks Using Macrocyclic Building Blocks. *Angew. Chem., Int. Ed.* **2020**, *59*, 275–280.

41. Bhangu, S. K.; Charchar, P.; Noble, B. B.; Kim, C.-J.; Pan, S.; Yarovsky, I.; Cavalieri, F.; Caruso, F. Origins of Structural Elasticity in Metal–Phenolic Networks Probed by Super-Resolution Microscopy and Multiscale Simulations. *ACS Nano*, **2021**. (DOI: 10.1021/acsnano.1c08192)

42. Sever, M. J.; Wilker, J. J. Visible Absorption Spectra of Metal–Catecholate and Metal–Tironate Complexes. *Dalton Trans.* **2004**, 1061–1072.

43. Lin, Z.; Zhou, J.; Cortez-Jugo, C.; Han, Y.; Ma, Y.; Pan, S.; Hanssen, E.; Richardson, J. J.; Caruso, F. Ordered Mesoporous Metal–Phenolic Network Particles. *J. Am. Chem. Soc.* **2020**, *142*, 335.

44. Kim, Y. S.; Liu, M.; Ishida, Y.; Ebina, Y.; Osada, M.; Sasaki, T.; Hikima, T.; Takata, M.; Aida, T. Thermoresponsive Actuation Enabled by Permittivity Switching in an Electrostatically Anisotropic Hydrogel. *Nat. Mater.* **2015**, *14*, 1002–1007.

45. Song, J. E.; Cho, E. C. Dual-Responsive and Multi-Functional Plasmonic Hydrogel Valves and Biomimetic Architectures Formed with Hydrogel and Gold Nanocolloids. *Sci. Rep.* **2016**, *6*, 1–10.

46. Zhang, W.; Besford, Q. A.; Christofferson, A. J.; Charchar, P.; Richardson, J. J.; Elbourne, A.; Kempe, K.; Hagemeyer, C. E.; Field, M. R.; McConville, C. F.; Yarovsky, I.; Caruso, F. Cobalt-Directed Assembly of Antibodies onto Metal-Phenolic Networks for Enhanced Particle Targeting. *Nano Lett.* **2020**, *20*, 2660–2666.

47. Rahim, A. M.; Björnmalm, M.; Bertleff-Zieschang, N.; Besford, Q.; Mettu, S.; Suma, T.; Faria, M.; Caruso, F. Rust-Mediated Continuous Assembly of Metal–Phenolic Networks. *Adv. Mater.* **2017**, *29*, 1606717.

48. Nagy, J. A.; Herzberg, K. T.; Masse, E. M.; Zientara, G. P.; Dvorak, H. F. Exchange of Macromolecules between Plasma and Peritoneal Cavity in Ascites Tumor-Bearing, Normal, and Serotonin-Injected Mice. *Cancer Res.* **1989**, *49*, 5448–5458.

49. Fragasso, A.; De Franceschi, N.; Stommer, P.; van der Sluis, E. O.; Dietz, H.; Dekker, C. Reconstitution of Ultrawide DNA Origami Pores in Liposomes for Transmembrane Transport of Macromolecules. *ACS Nano* **2021**, *15*, 12768.

50. Park, H. B.; Kamcev, J.; Robeson, L. M.; Elimelech, M.; Freeman, B. D. Maximizing the Right Stuff: The Trade-Off between Membrane Permeability and Selectivity. *Science* **2017**, *356*, eaab0530.

51. Kim, C.-J.; Ercole, F.; Ju, Y.; Pan, S.; Chen, J.; Qu, Y.; Quinn, J. F.; Caruso, F. Synthesis of Customizable Macromolecular Conjugates as Building Blocks for Engineering Metal–Phenolic Network Capsules with Tailorable Properties. *Chem. Mater.* **2021**, *33*, 8477–8488.

52. Martinez-Finley, E. J.; Gavin, C. E.; Aschner, M.; Gunter, T. E. Manganese Neurotoxicity and the Role of Reactive Oxygen Species. *Free Radicals Biol. Med.* **2013**, *62*, 65–75.

53. Riemschneider, S.; Herzberg, M.; Lehmann, J. Subtoxic Doses of Cadmium Modulate Inflammatory Properties of Murine RAW 264.7 Macrophages. *BioMed Res. Int.* **2015**, *2015*, 295303.

54. Gause, K. T.; Yan, Y.; O'Brien-Simpson, N. M.; Cui, J.; Lenzo, J. C.; Reynolds, E. C.; Caruso, F. Codelivery of NOD2 and TLR9 Ligands via Nanoengineered Protein Antigen Particles for Improving and Tuning Immune Responses. *Adv. Funct. Mater.* **2016**, *26*, 7526–7536.

55. Cui, J.; De Rose, R.; Best, J. P.; Johnston, A. P.; Alcantara, S.; Liang, K.; Such, G. K.; Kent, S. J.; Caruso, F. Mechanically Tunable, Self-Adjuvanting Nanoengineered Polypeptide Particles. *Adv. Mater.* **2013**, *25*, 3468–3472.

56. Sexton, A.; Whitney, P. G.; Chong, S.-F.; Zelikin, A. N.; Johnston, A. P.; De Rose, R.; Brooks, A. G.; Caruso, F.; Kent, S. J. A Protective Vaccine Delivery System for In Vivo T Cell Stimulation Using Nanoengineered Polymer Hydrogel Capsules. *ACS Nano* **2009**, *3*, 3391–3400.

57. Chong, S. F.; Sexton, A.; De Rose, R.; Kent, S. J.; Zelikin, A. N.; Caruso, F. A Paradigm for Peptide Vaccine Delivery Using Viral Epitopes Encapsulated in Degradable Polymer Hydrogel Capsules. *Biomaterials* **2009**, *30*, 5178–86.

58. Lau, A. C.; Wu, C. Thermally Sensitive and Biocompatible Poly(*N*-Vinylcaprolactam): Synthesis and Characterization of High Molar Mass Linear Chains. *Macromolecules* **1999**, *32*, 581–584.

59. Seuring, J.; Agarwal, S. First Example of a Universal and Cost-Effective Approach: Polymers with Tunable Upper Critical Solution Temperature in Water and Electrolyte Solution. *Macromolecules* **2012**, *45*, 3910–3918.

Table of Content Graphic